Atmospheric Environment 75 (2013) 15–23

Contents lists available at SciVerse ScienceDirect

Atmospheric Environment

journal homepage: www.elsevier.com/locate/atmosenv

Effect of water vapour condensation on the radon content in subsurface air in a hypogeal inactive-volcanic environment in Galdar cave, Spain

A. Fernandez-Cortes [a,*], D. Benavente [b], S. Cuezva [b], J.C. Cañaveras [b], M. Alvarez-Gallego [a], E. Garcia-Anton [a], V. Soler [c], S. Sanchez-Moral [a]

[a] Depto. Geología, MNCN-CSIC, C/José Gutiérrez Abascal, n.2, 28006 Madrid, Spain
[b] Depto. Ciencias Tierra y Medio Ambiente, Universidad de Alicante, 03080 Alicante, Spain
[c] Estación Volcanológica de Canarias, IPNA-CSIC, 38206 La Laguna, Tenerife, Spain

HIGHLIGHTS

- We monitored the weather-driven processes controlling gas exchange on subsurface.
- Anomalies on radon signal were statistically clustered.
- Relative humidity over 70% triggers the vapour effective condensation (EC).
- Reduction of air-filled porosity of rock by EC hides the radon exchange by diffusion.
- Microclimatic conditions were parameterized to predict radon concentration anomalies.

ARTICLE INFO

Article history:
Received 30 July 2012
Received in revised form
6 April 2013
Accepted 11 April 2013

Keywords:
Radon anomalies
Vapour condensation
Gas diffusion
Underground cavities
Subsoil monitoring

ABSTRACT

Fluctuations of trace gas activity as a response to variations in weather and microclimate conditions were monitored over a year in a shallow volcanic cave (Painted Cave, Galdar, Canary Islands, Spain). ^{222}Rn concentration was used due to its greater sensitivity to hygrothermal variations than CO_2 concentration. Radon concentration in the cave increases as effective vapour condensation within the porous system of the rock surfaces inside the cave increases due to humidity levels of more than 70%. Condensed water content in pores was assessed and linked to a reduction in the direct passage of trace gases. Fluctuations in radon activity as a response to variations in weather and microclimate conditions were statistically identified by clustering entropy changes on the radon signal and parameterised to predict radon concentration anomalies. This raises important implications for other research fields, including the surveillance of shallow volcanic and seismic activity, preventive conservation of cultural heritage in indoor spaces, indoor air quality control and studies to improve understanding of the role of subterranean terrestrial ecosystems as reservoirs and/or temporary sources of trace gases.

1. Introduction

In volcanic near-surface subterranean systems, by studying variations in the flux of trace gases as radon (^{222}Rn) across the soil/rock–air interface, certain geodynamic processes associated with shallow volcanic activity can be assessed (Eff-Darwich et al., 2002; Viñas et al., 2007; among others). However, anomalies in trace gas concentrations caused by geological events may be hindered by or present irregularities due to certain physical and meteorological factors. Other studies that consider the temporal variations of radon in caves, tunnels and bore-holes focus mainly on the convective processes induced by inside/outside temperature differences and variations in atmospheric pressure (Fernandez-Cortes et al., 2009; Kowalczk and Froelich, 2010; Perrier and Richon, 2010; among others).

The gaseous exchange between surface/underground and atmosphere is linked to the presence of pores, macro-pores and subsurface cavities, which act as storage and/or temporary sources of radon (^{222}Rn), CO_2, H_2O_v and CH_4. Thus, a similar pattern of CO_2 and Rn gas exchange, as controlled by the degree of moisture

* Corresponding author. Tel.: +34 914111328 1178; fax: +34 915644740.
E-mail addresses: acortes@mncn.csic.es (A. Fernandez-Cortes), david.benavente@ua.es (D. Benavente), scuezva@ua.es (S. Cuezva), jc.canaveras@ua.es (J.C. Cañaveras), mag@mncn.csic.es (M. Alvarez-Gallego), elena.garcia@mncn.csic.es (E. Garcia-Anton), vsoler@ipna.csic.es (V. Soler), ssmilk@mncn.csic.es (S. Sanchez-Moral).

1352-2310/$ – see front matter © 2013 Elsevier Ltd. All rights reserved.
http://dx.doi.org/10.1016/j.atmosenv.2013.04.030

present in the pore and fissure system in the external soil and epikarst, has been described for very stable subterranean atmospheres under vapour-equilibrium pressure near saturation (Cuezva et al., 2011; Fernandez-Cortes et al., 2011).

Subsurface trace gases may be divided into three states: in caves/voids and pore air, dissolved in pore water, and attached by sorption to soil grains (Nazaroff, 1992). In particular, a portion of radon content of pore air is then exhaled from the pore space into microcracks, fractures and the cave atmosphere, mainly by molecular diffusion or advective transport, due to differences in air pressure between the air that fills the cave and the porous rock that surrounds it. Diffusion-induced subsurface radon movement is notable in capillaries and small-pored rocks, compared with advection transport that may play an exclusive role in larger pores or fractured media (Etiope and Martinelli, 2002).

In this paper, water condensation in porous volcanic materials is studied in detail in order to understand the variation in and anomalous levels of radon gas in a shallow cave (Painted Cave, Galdar, Canary Islands, Spain). This is a suitable study site, as it is isolated from direct rainfall and solar radiation, air ventilation with the outer atmosphere is restricted by an artificial barrier, and there is no upper soil cover, which means that the gas exchange between subsurface-atmosphere is mainly limited through the homogeneous volcanic host-rock with a condensable pore structure. We test the hypothesis that condensation/evaporation cycles in inner substrates of host-rock govern the short-term and seasonal isolation and opening of the subterranean atmosphere and, consequently, play a key role in the gas exchange with the outer atmosphere. The cave's microclimate and weather conditions were monitored exhaustively, gas anomalies were statistically identified by clustering the changes in gas signal entropy, and a detailed study of effective condensation was carried out in terms of microclimate conditions and pore structure properties.

2. Materials and methods

2.1. Site and rock description

The town of Galdar is located on the subtropical latitudinal belt with a Mediterranean pluviseasonal-oceanic climate. The Painted Cave is part of a larger complex of six caves that were excavated in the volcanic toba by the island's former inhabitants. The cave complex of Galdar was settled at 99 m above sea level in an isolated volcanic geological structure located well above the current water table. The host rock of the cave complex outcrops without any covering soil layer, and is a sequence of high porous pyroclastic layers (lapilli tuff) with an average thickness of 10–40 cm and softer mm-thick beds (Sanchez-Moral et al., 2002). The volcanic host-rock has a complex porous media: high values of porosity (~36%, with high proportion of connected porosity (28%) and polymodal pore-size distribution (Benavente et al., 2009). Tuff presents two important fractions of small pores in the pore radius ranges of 1 nm–0.01 μm and 0.1–1 μm, which are related to pyroclastic minerals such as zeolites, micritic calcite and argillaceous minerals. The largest pores are defined by pyroclasts in ranges of 1–10 μm and 0.1 μm–1 mm which should therefore favour pore fluid displacement.

The monitoring site is a rectangular decorated chamber (159 m^3) excavated in the host rock (Fig. 1) with the ceiling (average thickness of 2.4 m), floor and three walls of tuff and an artificial, non-airtight closure near the built exterior. The study site is isolated from direct rainfall and solar radiation by a raised structure made from aluminium with polyurethane foam insulation covering an area of 5500 m^2, including the complete footprint of the cave on the surface. This construction is not closed off by any walls, allowing for partial ventilation from surface air. A concrete wall also surrounds the archaeological complex to avoid runoff from allochthonous water. These features make Galdar cave a unique subterranean laboratory in volcanic rock and the conditions help to simplify the study as water vapour is the only source of water supply, and therefore the only hydrological factor to consider.

2.2. Micro-environmental monitoring system and time series analysis

The subterranean laboratory has an eleven-sensor network designed for the narrow range of measurements of air and rock-surface parameters: temperature, relative humidity, and carbon dioxide and radon (^{222}Rn) content. Data were collected every 5 min over a period of 13 months (1/03/2004–31/03/2005) using a

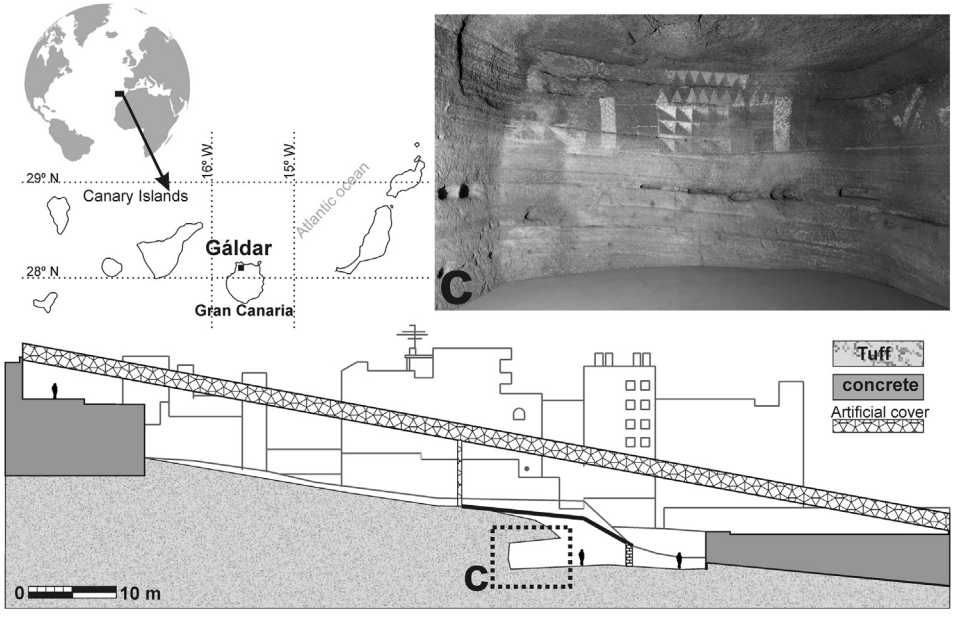

Fig. 1. Location and cross-section of the volcanic outcrop of the Galdar cave complex. C: View of inner surfaces of the Galdar cave.

dataTaker DT50 data logger (Thermo Fisher Scientific Australia Pty Ltd). Temperatures were measured in the air and on the rock surface of inner walls and the ceiling (interface rock–air) using a resistance thermometer Pt100 1/10 DIN (measuring range 0–50 °C, accuracy ±0.03 °C and resolution 0.01 °C at 0 °C). Humidity data were obtained using a HygroClip S3 capacitive sensor (Rotronic-Switzerland; measuring range 0–100% RH and accuracy ±0.6%). Cave air CO_2 concentration was measured using NDIR technology (model 8102, Ventostat) over the 0–7000 ppm range, with an accuracy of 7% or ±75 ppm. The ^{222}Rn concentration of air was registered using a Pylon AB5 scintillator–photomultiplier detector and PRD sensor (Pylon Electronic Inc., Canada), with a lowest detectable activity of 24.8 Bq m^{-3}, a sensitivity of 0.041 cpm (Bq m^{-3})$^{-1}$, accuracy of ±4% and nominal background of 0.4 cpm. Air sensors were located at 1 m above cave floor and 1 m far from cave walls. Daily air pressure data were obtained from a weather information service provided by AEMET-Spain from the Gando meteorological station (Gran Canaria airport; 27°56′N, 15°23′W, 23 m a.s.l., and 35.4 km from Galdar).

The entropy of curves technique (Denis and Cremoux, 2002) is a suitable statistically based method to cluster the short-term and seasonal variability of environmental data over periods of time. This technique makes it possible to divide a non-stationary random field, such as radon activity over periods of time, into periods where the data are stationary (constant entropy) or can be rendered thus by trend elimination. Entropy, $H(t)$, is a measure of uncertainty and variability; the larger the variability, the greater the entropy. Variations in the entropy value of radon series reveal changes in the degree of influence of a certain environmental parameter, and thus also allow the boundaries of periods with anomalous concentrations to be defined. The radon signal was segmented by applying the entropy of curves technique, and a non-parametric Kendall's test (Helsel et al., 2006) was then used to ascertain the correlation of environmental data, in particular the cause–effect relationship between the radon signal and several environmental parameters or factors (relative humidity or air density differences).

3. Results and discussion

3.1. Environmental parameters and trace gas concentration

Fig. 2A shows the evolution over time of the thermo-hygrometric conditions inside the Galdar cave (air and rock surface from walls and ceiling) over an annual cycle (2004–2005) relative to the external weather conditions. The annual average temperature outside the cave was 19.65 °C, and the average relative humidity was 68.62%, with monthly values ranging from 55.9% (January) to 75.8% (June). The intense evaporation rate due to the nearby ocean during summer determines both high monthly temperatures (>20 °C) and relative humidity values (>70%) from June to October. Rainfall was 561 mm year^{-1} and occurred mainly in spring (74.5% from February to May) and autumn (23.5% from September to December). No rain fell directly on the Painted Cave complex, as it was isolated by the cover described above.

Inside the cave, the annual average air temperature was 21.11 °C. Monthly air temperatures registered the same seasonal pattern as for the exterior, but with shorter annual amplitude (±Δ5.62 °C) and smoother mean daily fluctuations (±Δ0.27 °C). From October to May, average monthly air temperature values inside the cave clearly remained +1.0 °C higher than outside, reaching up to +2.7 °C between December and February. However, daily temperature fluctuations and relative humidity outside the cave (averaged at ±Δ5.32 °C and ±30.4% over the year) favoured short-term thermal inversion for the same period, especially during winter and early spring. Annual relative humidity inside the cave averaged 62.4%, ranging from 37.9% (January) to 74.0% (August).

The rock-surface temperature at cave's ceiling is almost equal to walls temperature during the period monitored. The air temperature relationship between cave air and rock surface (walls and ceiling) can be divided into three periods in an annual cycle: A) from early June to November, when the air is at a higher temperature than the rock surface (reaching a difference of +1.9 °C in August, considering monthly averages); B) from December to February, when the temperature gradient is reversed up to approximately −1.0 °C (February); and C) from March to the end of May, with differences lower than ±0.5 °C between the two temperatures.

Natural variations in carbon dioxide levels (excluding short-term increases due to the presence of visitors inside the cave) did not show a remarkable accumulation or any seasonal variation. The mean carbon dioxide concentration was 389 ppmv, practically the average atmospheric concentration, with maxima below 418 ppmv over the entire monitoring period. The absence of a soil layer above the cave acting as source of CO_2 leads to this pattern over time for this trace gas, in contrast to radon (^{222}Rn), which emanates continuously from the host-rock. The analysed time series of radon concentration in cave air is shown in Fig. 2B, which also shows the stationary segments of the radon signal characterised by constant entropy. The average radon concentration was 92 Bq m^{-3}, with a minimum of 85 Bq m^{-3} and a maximum of 120 Bq m^{-3}. The mean monthly radon signal values range from 87 Bq m^{-3} (January) to 103 Bq m^{-3} (August). Daily variations in radon concentration were scarce (mean of 2 Bq m^{-3}) but some short-term fluctuations lasting several days were registered, particularly in the summer (in August, for example, total radon signal amplitude reaches 24 Bq m^{-3}). This annual radon cycle has been regularly recorded each year since the site acquired its current conditions (i.e. with the artificial cover described above isolating the Painted Cave).

3.2. Pattern of ^{222}Rn and relative humidity

The low radon levels recorded in the cave are the results of the large and continuous air exchange with the outer atmosphere. However, any fluctuation or outlier data regarding the background level (approximately the average radon concentration level) may indicate either the influence of weather and microclimate conditions in the cave on gas exchange, or certain correlations between gas emissions and the shallow volcanic and/or seismic activity. However, during the period studied (March 2004–April 2005), no volcanic activity or seismic events were recorded by the nearest two stations (Guía and Osorio, located 3.1 km and 12.7 km from Galdar village) in the Canary Islands Volcanic and Seismic Monitoring Network, run by Spanish 'Instituto Geográfico Nacional' (IGN). Similarly, the IGN seismic catalogue recorded no earthquake activity in a 25-km square centred on the study site.

Over an annual cycle, radon concentration levels are below the annual average during the colder months (December to end of May), and fluctuate at around the annual average during the summer months, except from the end of July to August, when the average daily concentration of radon reaches 120 Bq m^{-3}. As shown in Fig. 2A and B, this period is a stationary segment with maximum entropy (approximately 2–4 times higher than all other segments) and, consequently, maximum variability in radon concentration. These anomalies in the radon signal were coeval to a period in which relative humidity was above the average annual value and the air temperature inside the cave was always higher than the temperature at the rock surface of the walls and ceiling, and some sharp weather fluctuations were recorded, causing a disturbance of the thermo-hygrometric equilibrium between the cave air and the

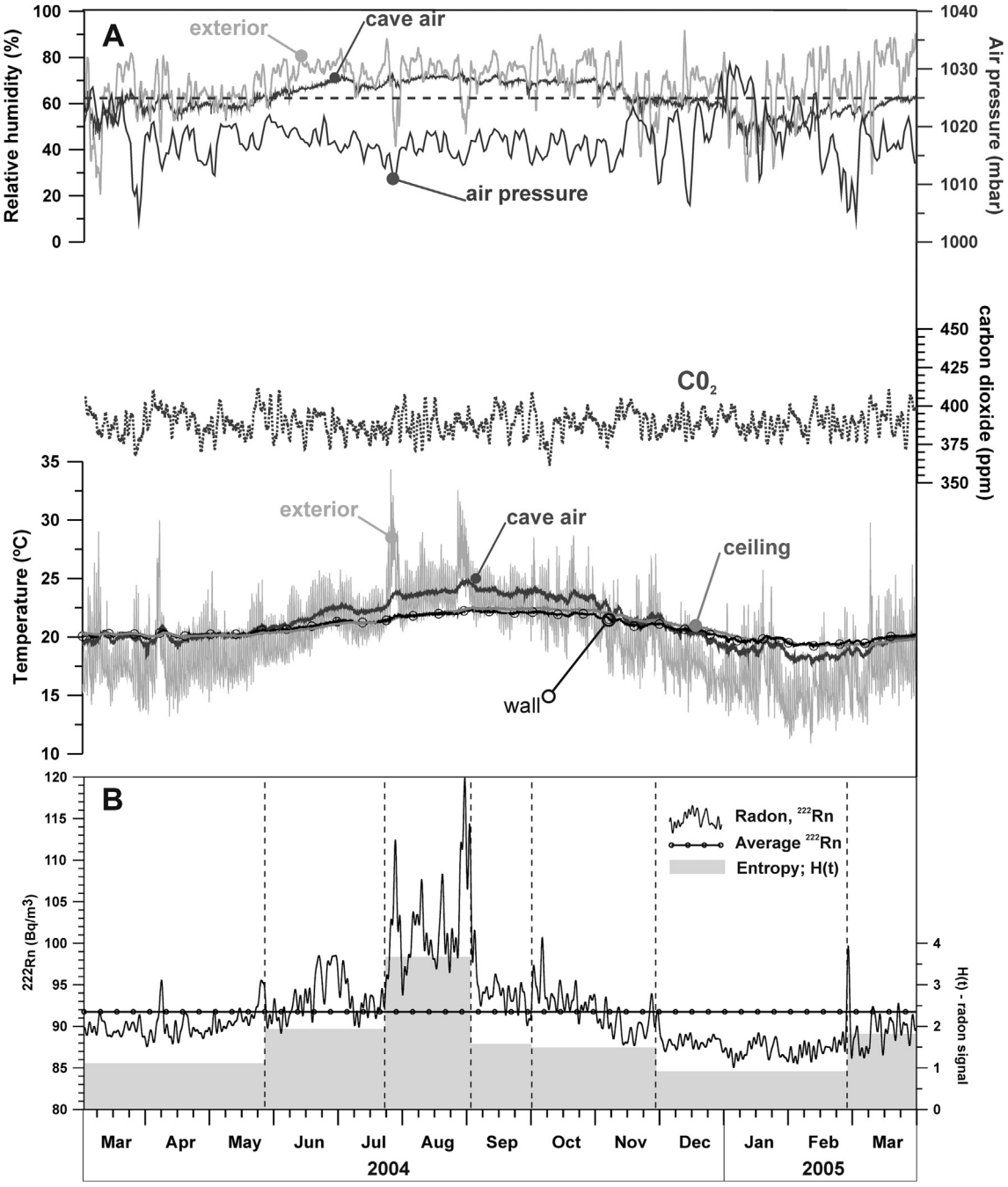

Fig. 2. A: Thermo-hygrometric conditions inside Galdar over an annual cycle (2004–2005) relative to the exterior meteorological conditions. Dashed red line shows the annual average of relative humidity of cave air. B: Time series of radon concentration in cave air (^{222}Rn, Bq m^{-3}) and average concentration (2004–2005). Dashed lines delimit several statistically homogeneous and stationary clusters (constant entropy), or potentially so after detrending (see text).

exterior atmosphere. The most notable anomalies in the radon signal were registered in August, which is the only month when the average monthly temperature of the exterior air is higher (+0.4 °C) than the cave air, and the relative humidity of the air inside the cave reached a peak and remained above 70%.

The lower proportion of larger pores and the absence of significant fractures in the host-rock connected to deeper areas below the cave indicate that radon transport to the atmosphere in the cave occurs mainly by diffusion. Transport by advection is negligible, as there is no notable pressure gradient between the cave's atmosphere and the air-filled porous rock. The small size of this shallow cave therefore involves a barometric equilibrium between the hypogeal environment, the outer atmosphere and the surrounding rock. Only short-term and seasonal air-density gradient inversions, caused by falling exterior temperatures, occur between the cave and the external atmosphere, and which influence ventilation, as discussed further below.

The mean vapour-adsorption curve obtained for several fresh/unweathered samples of tuff from the volcanic outcrop at Galdar (Fig. 3A) revealed a bend at a relative humidity of about 70–75%, from which the amount of adsorbed water (expressed as $\Delta m/m_0$) increases significantly (Benavente et al., 2009). The exponential growth rate of vapour-adsorption from this HR(%)-threshold ($[HR]_t$) is related to an increase in water films on the surface layer of

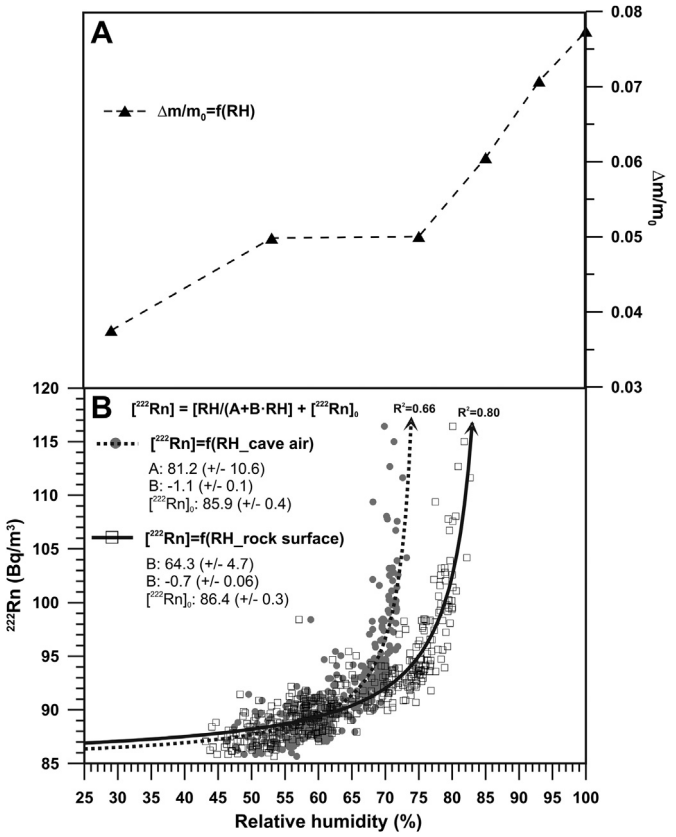

Fig. 3. A: Mean water adsorption curve of the host-rock at different relative humidities (RH); $\Delta m/m_0 = f(\mathrm{RH})$ (from Benavente et al., 2009), and B: Daily-averaged relationship of radon concentration in cave air (^{222}Rn, Bq m^{-3}), relative humidity of cave air (red line) and ceiling rock-surface (blue line).

rock-surface pores, and consequently the beginning of capillarity water condensation.

Condensation is a dynamic process involving the flow of water vapour between the air and a solid surface. The flow varies with time and involves alternating condensation and evaporation of water depending on the direction of the vapour gradient between the air and the surface. Effective condensation occurs when vapour pressure in the air is higher than on the rock surface, which is corrected by the threshold of relative humidity, above which water condensation is more active due to the presence of a pore structure and dissolved salts. Derivations of effective condensation equations are shown in Appendix A, and a critical relative humidity of 75% is considered for the calculations.

Once the condensation process is triggered on the cave's ceiling and walls, the initial amount of water available for condensation is crucial in terms of ^{222}Rn diffusion through the rock, which depends on the microclimate conditions, pore structure and pore water of the host-rock. The diffusivity of radon into the cave atmosphere is markedly hampered once the rock pore volume becomes saturated with condensed water. The diffusive movement is described by Fick's law, for which gas flux is directly related to the concentration gradient and to a constant molecular diffusion coefficient Dm (m^2 s^{-1}). For a specific gas, Dm only changes with temperature, pressure and the physical nature of the substance through which the molecular motion takes place. In porous rocks, pore space presents a complex pore size distribution and connectivity and is generally filled up by water or air (or gas mixture). Thus, for each gas, the diffusion in liquid water (Dw) can be distinguished from the diffusive movement in air (Dm). In the absence of liquid water transport, ^{222}Rn presents a mean Dw of $1.37\cdot10^{-5}$ cm^2 s^{-1} and Dm of 0.12 cm^2 s^{-1} (Etiope and Martinelli, 2002), so radon diffusion in air is ~104 time faster than in water at room temperature. It means that ^{222}Rn may cover in liquid water just ~21 cm in a year. As a result, condensed water obstructs the direct passage of gases and it could modify the gas diffusion coefficients. The observed radon behaviour is in agreement with other studies, thus Papachristodoulou et al. (2007) observed that, once the soil pore volume becomes saturated to values above similar to 20%, the diffusion of radon was markedly hampered. Recently, Prasad et al. (2012) found the radon diffusion coefficients in loam soils vary from 9.60 × 10−6 m^2 s^{-1} to 1.27 × 10^{-7} m^2 s^{-1} with increasing water saturation from 0.4 to 0.82 due water saturation of the soil pores. Fig. 3A shows the behaviour of radon activity in the cave atmosphere (^{222}Rn in Bq m^{-3}) under variable moisture conditions of cave air and rock surface at the ceiling (expressed as RH%). Data for the relative humidity of the air–rock interface were obtained by assuming a dynamical equilibrium between vapour pressures of the air and the rock surface, depending on the temperature fluctuations of both microenvironments. Radon activity in the air is higher, as relative humidity increases both in the cave air and on the rock surface. This upward trend of radon content is linear within a RH range from 40 to 70%. From a relative humidity of 70–75%, the radon content of air undergoes a notable increase alongside relative humidity, in terms of both the air and the rock surface. The break point indicating the exponential increase of radon is close to 75% of relative humidity at the rock surface. This RH-value matches the break point of the water adsorption curve of the host-rock (expressed as a rate $\Delta m/m_0$), indicating a clear relationship between the beginning of capillarity water condensation on the rock surface and the rapid increase of radon levels in the cave atmosphere. Once Kendall's non-parametric test confirmed relative humidity as the key factor with a notable influence on variations of radon activity (best cause-effect correlation), a modified hyperbola ($y = [x/(A + B^*x)] + C$, with both horizontal and vertical asymptotes parallel to their coordinate axes; x and y) was used to simulate radon activity using relative humidity:

$$[^{222}\mathrm{Rn}] = [\mathrm{RH}/(A + B\cdot\mathrm{RH}] + [^{222}\mathrm{Rn}]_0 \quad (1)$$

where RH is the relative humidity (%), [^{222}Rn] is the radon activity (Bq m^{-3}) and A, B and $C = [^{222}\mathrm{Rn}]_0$ are coefficients defining the asymptotes.

For Eq. (1), the coefficient B is < 0, so the corresponding function graph shows two sides separated by a vertical asymptote. The left side of Eq. (1) was fitted to predict radon activity (Bq m^{-3}) as a function of the daily-average relative humidity of the cave air and the rock surface at the ceiling (%) (Fig. 3B). A better fit is achieved if the relative humidity of the rock surface is considered as the independent variable ($R^2 = 0.80$ with a standard deviation of the fitting, σ, equal to 2.14) instead of the relative humidity of cave air ($R^2 = 0.66$ and $\sigma = 2.80$). Chi-square coefficient, χ^2, is 393 for both fitted equations, which confirms that the radon activity estimated by these functions is consistent with the experimental data at the 0.05 significance level (α) according to the chi-square test (a χ^2 in the vicinity of 440, leading to a $\alpha = 0.05$, could question the consistency of the estimated values). In addition, the normalized chi-squared statistic, χ^2_{red}, is equal to 1 for both fitting models, so it indicates that the extent of the match between observations and estimates is in accord with the error variance and, therefore, it is a good fit. This indicates the key influence exerted by the moisture conditions of the rock surface porous system on increased radon activity in the cave atmosphere. The coefficient $[^{222}\mathrm{Rn}]_0$ determines the asymptotic level of radon activity for very low relative humidity, both in the air and on the rock surface. This $[^{222}\mathrm{Rn}]_0$ value

(approximately 86 Bq m^{-3} in both cases) should correspond with the background level for radon emissions with no shallow volcanic activity, and once the masking effect due to the isolation of cave atmosphere by vapour condensation in the inner rock surfaces is removed. The ratio A/|B| represents a vertical asymptotic level of relative humidity (on daily average) of both the air (76.1%) and on the rock surface (86.7%) close to what would be expected for maximum anomalous levels of radon in the cave atmosphere.

3.3. Estimation of ^{222}Rn levels by changes in the climate and microclimate conditions

Fig. 4A shows the daily-averaged signal of air radon activity in relation to the condensed water adsorbed by the ceiling rock surface. Effective condensation (expressed as gH_2O per m^3 of air and day) was calculated as a function of the temperature of the ceiling rock surface and assuming a dynamic equilibrium between vapour pressure of air and rock surface. Cave air radon levels were simulated using Eq. (1) over an annual cycle as a function of the relative humidity calculated for the rock surface at the ceiling (Fig. 4A, dotted line). The simulated radon activity of cave air (Bq m^{-3}) is more consistent to the observed data if condensation (calculated from relative humidity changes in the rock surface) is considered as control parameter ($R^2 = 0.80$ with a standard deviation of the fitting, σ, equal to 2.14). By contrast, the fit becomes worse if the air density differences (exterior-interior) are considered ($R^2 = 0.58$, $\sigma = 3.11$), using both positive and negative air density differences and the best fitting function (inverse of straight line equation, plotted as dotted line in Fig. 5A). The effective vapour condensation on the surface porous layer of tuff covering the inner surfaces of the cave matches up with the highest radon fluctuations above its annual average (Fig. 4A). On the contrary, the background levels of radon are reached once vapour condensation is not triggered and the air-density gradient is reversed.

Radon anomalies can be inferred once the gas concentration is clearly above the average radon concentration (roughly 92 Bq m^{-3}), essentially delimited from the middle of June to the end of October. Effective condensation was triggered once the relative humidity of the cave air reached and remained close to 70% (air temperature; 21.6 °C), and was depleted once relative humidity dropped below this value (at 23.4 °C). Consequently, radon anomalies appeared when the rate of effective condensation on the ceiling rock surface rose above 150 g_{H_2O} m^{-3} day^{-1}, and were highest when effective condensation was higher than 300 g_{H_2O} m^{-3} day^{-1}. Maximum concentration of radon anomalies and water condensation experience an upward trend until the end of August. Although the radon contribution by diffusion from the host rock to the cave atmosphere is depleted, the isolation of the cave atmosphere also causes a drop in the bidirectional gas-phase exchange rate between the portion of air-filled porous rock and cave air. The isolation phenomenon of the cave resulting from saturation of the porous system due to water condensation is sufficient to concentrate the radon in the cave atmosphere. It thus remains at high and sometimes anomalous levels in relation to its background level or annual average concentration.

Local weather drives ventilation by differences in air density between the cave and the external atmosphere. Drops in temperature outside the cave can trigger density-driven flows, resulting in air exchanges between the cave and the atmosphere through the non-airtight closure, and a rapid decline of radon levels is consequently registered. These environmental conditions prevail in time (86.7% of the monitoring period), particularly from November to June, when exterior air density is higher than inside the cave. Therefore, the air renewal process keeps radon levels below the annual average concentration (Fig. 4B). Daily-averaged relationship between radon signal and air density differences exterior-interior is

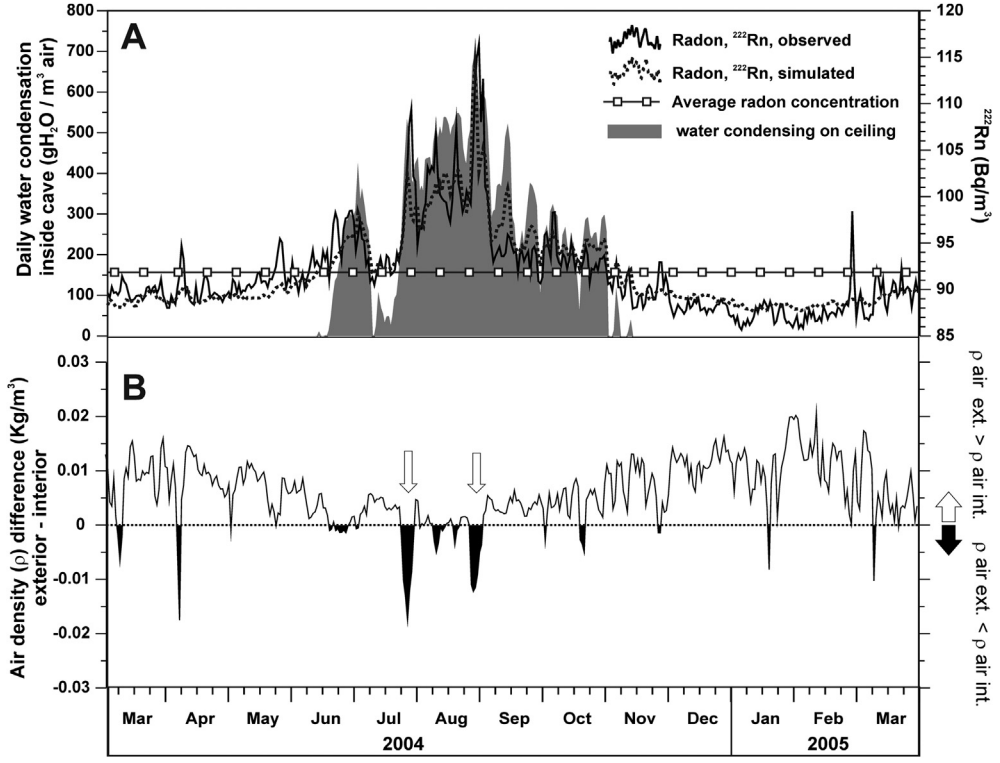

Fig. 4. A: Observed and simulated signal of radon activity in cave air (Bq m^{-3}) in relation to effective condensation (g of H_2O m^{-3} air and day, adsorbed by the ceiling rock surface) over an annual cycle (2004–2005). B: Time series of air density differences between the outer atmosphere and cave air (daily averaged). Daily-averaged relationship between radon concentration of cave air and various micro-environmental parameters.

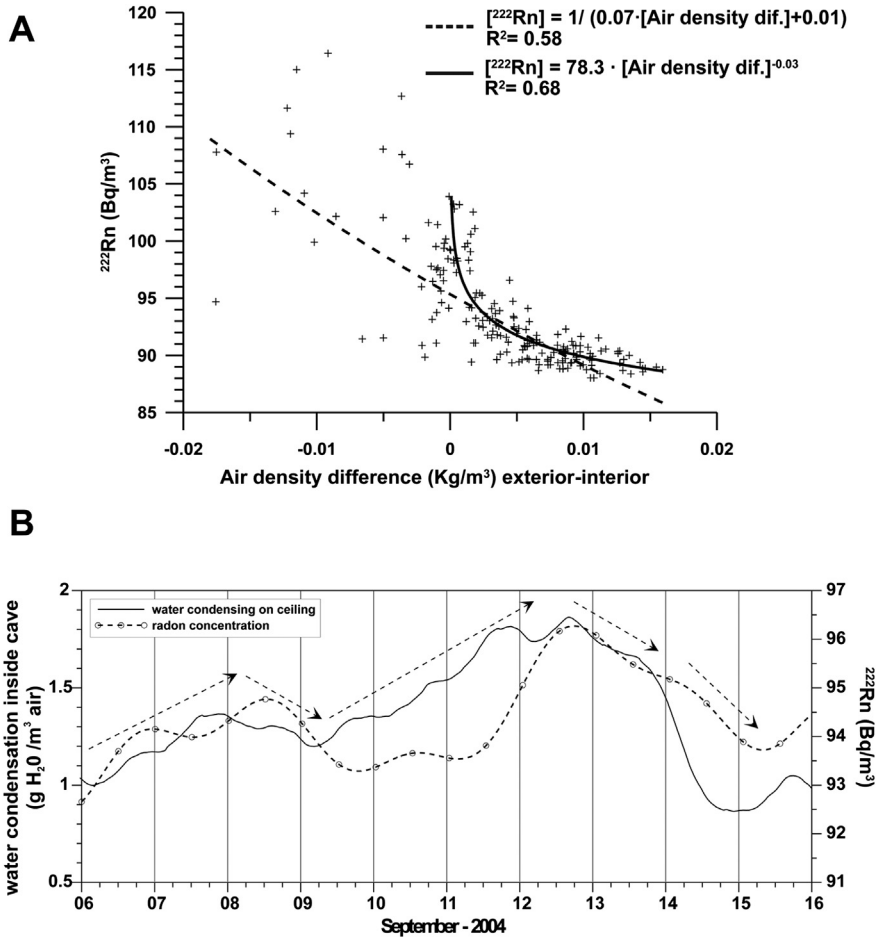

Fig. 5. A: Daily-averaged relationship between radon concentration air density differences between the outer atmosphere and cave air. B: Detailed plot of water condensation controlling the soft and short-term variations of radon activity, under favourable conditions for density-driven ventilation of cave: air density at exterior higher than inside the cave (dashed arrows show the prevailing trend of both parameters).

shown on Fig. 5A. Only the positive differences between both air densities (generally once daily average temperature at exterior is below 24.4 °C) entail a rapid drop on radon levels of cave air, while an inverse gradient of densities usually coincide with outliers on radon signal but without a remarkable functional relationship between both variables. Nevertheless, the soft fluctuations of radon concentration are coeval to the changes of water condensing on the inner rock surfaces of the cave, even under conditions that are favourable to density driven ventilation, e.g.: when air density is higher outside the cave than inside (Fig. 5B), which illustrates the effect of condensation inside the cave on the short-term variations of radon activity.

An opposite pattern is promptly registered during the summer period with maximum levels and variability (entropy) of the radon signal due to the isolation of the cave atmosphere by intense water condensation. The intermittent and sharp rises in temperature for a few days at the end of July and end of August (+6.3 °C and +4.1 °C, respectively) cause the highest density differences between cave air and atmosphere, and consequently the most notable radon increase of +14 Bq m^{-3} and +15 Bq m^{-3}, respectively (marked in Fig. 4B with white-filled arrows). During these short periods, the cave operates as a motionless atmosphere that plays no part in the aerodynamic exchange with the external atmosphere. Thus, thermal stratification of the air creates a static trap of warm and less dense air inside the cave that contributes to the gas entrapment process.

4. Conclusions

Besides the observations of radon transportation by molecular diffusion combined with advective flow induced by barometric pressure in subterranean environments, such us confined underground buildings, tunnels, volcanic galleries (lava tubes) and caves, this study shows that anomalies of ^{222}Rn concentration in other shallower subterranean environments could be also controlled by variations in thermo-hygrometric conditions. Radon anomalies recorded in the indoor air of the Galdar cave are mainly caused by the seasonal increase in vapour condensation within the porous system of the rock surfaces inside the cave. This leads to water adsorption of the porous rock surfaces and the isolation of the cave's atmosphere due to a reduction of air-filled porosity of the surface layers of host-rock on the walls and ceiling. The highest radon concentration coincides with the period of high relative humidity (summer), and consequently with the highest rate of effective condensation of water on the inner rock surfaces (mainly the cave's ceiling).

The properties of the host rock's pore structure, and particularly water condensation behaviour, reveal a relative humidity threshold for the cave air of 70–75%, from which the amount of water adsorbed by the porous surface system significantly increases. Once these boundary moisture conditions were recorded during the field monitoring, certain radon signal anomalies in the cave air were triggered. In this local context, future experimental research should

focus on assessing the radon exhalation rate at the rock surface by simulating the condensation process in host rock samples under controlled moisture conditions and increasing water content.

Correlations between gaseous emissions and dynamic transport or geodynamic processes are usually defined according to the fluctuations of radon activity from a background level using subterranean sites as monitoring laboratories, but without considering any effect of other external environmental parameters. Here, it is clear that the role of condensed water on porous rock surfaces as an insulating agent of hypogeal environments should be considered in order to avoid any misleading data interpretations, including those relating to studies aimed at assessing research topics such as shallow volcanic and/or seismic activity by radon surveillance.

Acknowledgements

This study was financed by the Gran Canaria Island Council and within the framework of the Spanish MEC projects CGL2010-17108, CGL2011-25494 and CGL2011-25162. This study was possible thanks to the kind support and help received from the managers and staff at the Galdar Painted Cave Museum and Archaeological Park.

Appendix A. Effective condensation

This appendix describes the procedure to calculate the effective condensation of water on a porous geological substrate (expressed in grams of water vapour condensed by cubic metre of air) as a function of the microclimate conditions and the properties of the porous system in the substrate (chiefly the shallow portion of the rock/soil surface). A theoretical approach is defined in order to calculate the amount of water condensing on an exposed rock/soil surface, depending on the evolution over time of the differences in vapour pressure between air and the rock/soil surface, and the control exerted by the porous system of the rock based on lab experiments to calculate water adsorption curves of rock/soil samples at different relative humidities.

Partial vapour pressure, P_v (in hPa or mbar), is related to relative humidity (RH) as follows:

$$\mathrm{RH}(\%) = (P_v/P_{vs})\cdot 100, \tag{A1}$$

where P_{vs} is the saturated vapour pressure (measured in hPa or mbar), which depends on air temperature (T in °C). In a saturated vapour condition with a planar surface of pure water at temperature T between −20° and 50 °C, Buck (1981) recommends the following well-known Magnus–Tetens formula:

$$P_{vs} = 6.1121\cdot\exp[(17.502\cdot T)/(240.97+T)]. \tag{A2}$$

The above equation relates the saturation vapour pressure (P_{vs}) of pure water to temperature; however, a slight correction must be made when dealing with moist air rather than pure water vapour. This correction, known as the enhancement factor $f(T,P)$, is a weak function of temperature and air pressure, P_0 (Buck, 1981), when multiplied to P_{vs};

$$f(T,P) = 1.01031 - 0.000869652\cdot T + 0.00000362121\cdot P_0. \tag{A3}$$

Similarly, P_{vs} can also refer to rock surface temperature, T_r, which is in thermal equilibrium with the thin air film immediately above, as follows;

$$P_{vs-rock} = 6.1121\cdot\exp[(17.368\cdot T_r)/(238.88+T_r)]. \tag{A4}$$

Absolute humidity (water vapour density), Ha, expressed as grams of vapour contained in a cubic metre of air, can be inferred from P_{vs} (or $P_{vs\text{-}rock}$), in mbar, considering the equation of state of a hypothetical ideal gas, as follows;

$$\mathrm{Ha}\left(\mathrm{g\ m^{-3}}\right) = m(\mathrm{H_2O})\cdot[(P_{vs}\cdot 106)/1.01325]/[\mathrm{R}\cdot(273.15+T], \tag{A5}$$

where $m(H_2O)$ is the molecular mass of water (18.01528 g mol^{-1}), R is the ideal, or universal, gas constant (82.05746 cm^3 atm K^{-1} mol^{-1}), and T is the air temperature in °C.

Water condensation is triggered when the partial pressure of vapour in the air, P_{vs}, exceeds the vapour pressure at the temperature of the rock surface, $P_{vs\text{-}rock}$, or at the temperature of the water film previously condensed on the rock surface (such a thin water film will quickly reach thermal equilibrium with the rock surface). The process of water adsorption onto an exposed rock surface depends on rock and solution temperatures, solution ion strength and the pore radius of the rock. In the equilibrium, variation in the chemical potentials of water film (aqueous solution), $d\mu_S$, and vapour, $d\mu_V$, should be equal and the Gibbs–Duhem equation can therefore be expressed as follows:

$$d\mu_S = V_S dP_S - S_S dT_s + RT_s d\ln a_{H_2O} = d\mu_v = RT_s \ln P_V, \tag{A6}$$

where V_S is the molar volume of the solution, P_S the solution pressure, P_v the vapour pressure, S_S the solution entropy, T_s the solution temperature (equal to T_r under thermal equilibrium with rock surface), R is the gas constant per mole and a_{H_2O} is the solution's water activity. At a constant temperature,

$$V_S\, dP_S + RT_s \ln a_{H_2O} = RT_s \ln P_V. \tag{A7}$$

In an unsaturated porous material such as the porous rock that covers the cave, the capillary pressure is negative and is controlled by the curvature, κ_{SV}, of the solution-vapour meniscus in the pore entry. In this situation, the pressure of the solution can be written as:

$$P_S = P_0 + \sigma_{SV}\kappa_{SV}, \tag{A8}$$

where P_0 is the ambient pressure and σ_{SV} is the interfacial energy between the solution and vapour. Thus, the expression for the derivative of the solution pressure is (see Flatt, 2002 for details):

$$dP_s = d(\sigma_{SV}\kappa_{LV}). \tag{A9}$$

Substituting Eq. (A9) for Eq. (A6) and integrating;

$$\int_0^{\sigma_{SV}\kappa_{SV}} V_L d(\sigma_{SV}\kappa_{SV}) + RT\int_0^{\ln a_{H_2O}} d(\ln a_{H_2O}) = RT\int_{\ln P_{VS}}^{\ln P_V} d(\ln P_V), \tag{A10}$$

where P_V is the vapour pressure and P_{VS} the saturated vapour pressure. In unsaturated porous materials, the pressures are usually not high enough to affect molar volumes (Zilberbrand, 1999; Benavente et al., 2004); the compressibility of the solution may therefore be negligible and Eq. (A10) can be integrated to obtain:

$$V_L\sigma_{SV}\kappa_{LV} + RT_s \ln a_{H_2O} = RT_s \ln(P_V/P_{VS}) \tag{A11}$$

If the interface is flat (no curvature effects), the first term on the left of Eq. (A11) is negligible, and the water activity in the solution depends only on relative humidity (Eq. (A1)).

If a meniscus with a wet-table surface and a cylindrical pore of radius r are supposed, the curvature of the solution-vapour

meniscus is $\kappa_{LV} = 2/r$. The vapour pressure in the porous rock surface can be thus written as follows:

$$P_v = P_{vs} \cdot a_{H_2O} \cdot \exp[(-2\sigma_{sv} V_s / RT_s) \cdot (1/r)] \quad (A12)$$

or expressed in terms of the relative humidity-threshold ($[RH]_t$)

$$[RH]/100 = a_{H_2O} \cdot \exp[(-2\sigma_{sv} V_s / RT_s) \cdot (1/r)] \quad (A13)$$

The relative humidity-threshold ($[RH]_t$) can also be inferred by assessing the water adsorption curves of the rock samples at different relative humidities obtained experimentally in the lab (see Franzen and Mirwald, 2004; Benavente et al., 2009; etc.). From Eq. (A13) it is inferred that, under steady state micro-environmental conditions (T_S constant), $[RH]_t$ rises as the pore radius increases. Therefore, P_{vs} at the rock surface ($P_{vs\text{-}rock}$) from Eq. (A4) must be corrected downward as a function of the relative humidity-threshold ($[RH]_t$) of Eq. (A13), in order to calculate the partial vapour pressure at the temperature of the rock surface from which the effective water vapour condensation is triggered ($P'_{vs\text{-}rock}$). This correction is easily performed as follows:

$$P'_{vs-rock} = P_{vs-rock} \cdot [RH]_t / 100 \quad (A14)$$

Similarly, absolute humidity at the rock surface under effective condensation conditions can be calculated by substituting $P'_{vs-rock}$ for Eq. (A5).

$$H_{a-rock}\left(g\ m^{-3}\right) = m(H_2O) \cdot \left[\left(P'_{vs-rock} \cdot 10^6\right) \Big/ 1.01325\right] \Big/ [R \cdot (273,15 + T_r)] \quad (A15)$$

Effective condensation remains active until the vapour pressure (PV) equalizes the saturated vapour pressure (P'_{vs}) in the porous rock surface, according to Eq. (A14) or, in other words, once relative humidity is below the threshold ($[RH]_t$) according to Eq. (A13). In conclusion, the vapour amount that can effectively condense (when $P_{vs} > P'_{vs-rock}$) on the rock surface (with a prevailing cylindrical pore of radius r) can be calculated in grams of water per cubic meter of air (CE, $gH_2O\ m^{-3}$) as follows:

$$CE\left(gH_2O\ m^{-3}\right) = H_a - H_{a-rock} \quad (A16)$$

Conversely, when $P_{vs} < P'_{vs-rock}$, water is likely to evaporate from the rock surface in an amount of $H_{a\text{-}rock} - H_a$ ($gH_2O\ m^{-3}$).

References

Benavente, D., del Garcia-Cura, M.A., Garcia-Guinea, J., Sanchez-Moral, S., Ordoñez, S., 2004. The role of pore structure in salt crystallisation in unsaturated porous stone. Journal of Crystal Growth 260, 532–544.

Benavente, D., Canaveras, J.C., Cuezva, S., Laiz, L., Sanchez-Moral, S., 2009. Experimental definition of microclimatic conditions based on water transfer and porous media properties for the conservation of prehistoric constructions: Cueva Pintada at Galdar, Gran Canaria, Spain. Environmental Geology 56, 1495–1504.

Buck, A.L., 1981. New equations for computing vapor pressure and enhancement factor. Journal of Applied Meteorology 20 (12), 1527–1532.

Cuezva, S., Fernandez-Cortes, A., Benavente, D., Serrano-Ortiz, P., Kowalski, A.S., Sanchez-Moral, S., 2011. Short-term CO2(g) exchange between a shallow karstic cavity and the external atmosphere during summer: role of the surface soil layer. Atmospheric Environment 45, 1418–1427.

Denis, A., Cremoux, F., 2002. Using the entropy of curves to segment a time or spatial series. Mathematical Geology 34 (8), 899–914.

Eff-Darwich, A., Martin-Luis, C., Quesada, M., de la Nuez, J., Coello, J., 2002. Variations on the concentration of ^{222}Rn in the subsurface of the volcanic island of Tenerife, Canary Islands. Radiation Measurements 43, 1429–1436.

Etiope, G., Martinelli, G., 2002. Migration of carrier and trace gases in the geosphere: an overview. Physics of the Earth and Planetary Interiors 129, 185–204.

Fernandez-Cortes, A., Sanchez-Moral, S., Cuezva, S., Canaveras, J.C., Abella, R., 2009. Annual and transient signatures of gas exchange and transport in the Castañar de Ibor cave (Spain). International Journal of Speleology 38, 153–162.

Fernandez-Cortes, A., Sanchez-Moral, S., Cuezva, S., Benavente, D., Abella, R., 2011. Characterization of trace gases' fluctuations on a 'low energy' cave (Castañar de Ibor, Spain) using techniques of entropy of curves. International Journal of Climatology 31, 127–143.

Flatt, R.J., 2002. Salt damage in porous materials: how high supersaturations are generated. Journal of Crystal Growth 242, 435–454.

Franzen, C., Mirwald, P.W., 2004. Moisture content of natural stone: static and dynamic equilibrium with atmospheric humidity. Environmental Geology 46, 391–401.

Helsel, D.R., Mueller, D.K., Slack, J.R., 2006. Computer Program for the Kendall Family of Trend Test. Report: 2005-5275. U.S. Geological Survey Scientific.

Kowalczk, A.J., Froelich, P.N., 2010. Cave air ventilation and CO_2 outgassing by radon-222 modelling: how fast do caves breathe. Earth and Planetary Science Letters 289, 209–219.

Nazaroff, W.W., 1992. Radon transport from soil to air. Reviews of Geophysics 30 (2), 137–160.

Papachristodoulou, C., Ioannides, K., Spathis, S., 2007. The effect of moisture content on radon diffusion through soil: assessment in laboratory and field experiments. Health Physics 92 (3), 257–264.

Prasad, G., Ishikawa, T., Hosoda, M., Sorimachi, A., Janik, M., Sahoo, S.K., Uchida, S., 2012. Estimation of radon diffusion coefficients in soil using an updated experimental system. Review of Scientific Instruments 83 (9). Article Number: 093503.

Perrier, F., Richon, P., 2010. Spatiotemporal variation of radon and carbon dioxide concentrations in an underground quarry: coupled processes of natural ventilation, barometric pumping and internal mixing. Journal of Environmental Radioactivity 101, 279–296.

Sanchez-Moral, S., Garcia-Guinea, J., Sanz-Rubio, E., Canaveras, J.C., Onrubia-Pintado, J., 2002. Mortars, pigments and saline efflorescence from Canarian pre-Hispanic constructions (Galdar, Grand Canary Island). Construction and Building Materials 16, 241–250.

Viñas, R., Eff-Darwich, A., Soler, V., Martin-Luis, M.C., Quesada, M.L., de la Nuez, J., 2007. Processing of radon time series in underground environments: implications for volcanic surveillance in the island of Tenerife, Canary Islands, Spain. Radiation Measurements 42, 101–115.

Zilberbrand, M., 1999. On equilibrium constants for aqueous geochemical reactions in water unsaturated soils and sediments. Aquatic Geochemistry 5, 195–206.

Web references

http://www.ogimet.com (last accessed 30.07.12.), provided by AEMET-Spain.

http://www.ign.es/ign/layoutIn/volcaFormularioCatalogo.do (last accessed 30.07.12.).